Journal of the Korea Institute of Applied Superconductivity and Cryogenics
Vol.8, No.2, (2006), pp.37~42

Breakdown Characteristics of Insulation Materials for a Termination of Power Transmission Class HTS Cable

Dong-Soon Kwag, Hyeon-Gweon Cheon, Jae-Hyeong Choi, Sang-Hyun Kim

Department of Electrical Engineering and Engineering Research institute, Gyeongsang National University

shkim@gsnu.ac.kr

Abstract-- **A research on several characteristics such as volume breakdown and surface discharge of insulators for a termination of power transmission class HTS cable was performed. We investigated the surface discharge of glass fiber reinforced plastic (GFRP) under air, cryogenic nitrogen gas and nitrogen gas media. The breakdown characteristics of these media were studied. Experimental results revealed that flashover voltage greatly depends on pressure, temperature, the kinds of insulating media and voltages, but it is slightly affected by shape and material of electrode. The breakdown voltage of liquid nitrogen, cryogenic nitrogen gas and nitrogen gas deeply depends on the shape and dimension of electrode, kinds of voltages and pressure. Moreover, the breakdown voltage of cryogenic nitrogen gas and flashover voltage of GFRP in the cryogenic nitrogen gas is also influenced by temperature and vapour-mist density of the gas.**

1. INTRODUCTION

The discovery of high temperature superconductor (HTS) operating at above 77 K in 1987 renewed interest in superconducting power generation and transmission. Especially, high temperature superconducting cable promises to transmit a large capacity of electric power with lower voltage and in a compact size [1], [2].

A termination is one of the essential components for HTS cable system and it is used for connecting a cryogenic superconducting power cable with a generator or transformer at room temperature. The termination must span a temperature range from 77 K to 300 K, so the composite insulation system of liquid nitrogen, gas and solid polymer were used. With this insulation system, there are usually had the occurring of discharge on the surface of solid insulator and breakdown in the liquid nitrogen or gas. Nowadays, the termination is developing elsewhere in the world [3]-[5]. In Korea, KERI and LS Cable Ltd. are developing 154 kV class HTS power cable, to make the basic knowledge and data for insulation design of the termination the study on breakdown characteristic of insulators for the 154 kV class HTS cable is needed.

The structure of the 154 kV class terminations that is developing in Korea is shown in Fig. 1. The termination insulation is a three-layer structure consisting of nitrogen gas (GN_2), cryogenic-nitrogen gas (CGN_2) and liquid nitrogen (LN_2). Since the dielectric strength of nitrogen gas is low, the current lead is insulated with Glass Fibre Reinforced Plastic (GFRP) for reinforcing the dielectric strength.

From the Fig. 1, there are four breakdown channels that must be studied before insulation design of termination performed. They are labeled with (A), (B), (C) and (D) to correspond with the following terminology

(A) High voltage shielding-to-ground (surface discharge of GFRP in air)
(B) Current lead-to- ground (surface discharge of GFRP in GN_2)
(C) Current lead-to-ground (surface discharge of GFRP in CGN_2)
(D) Current lead-to-ground (breakdown in LN_2)

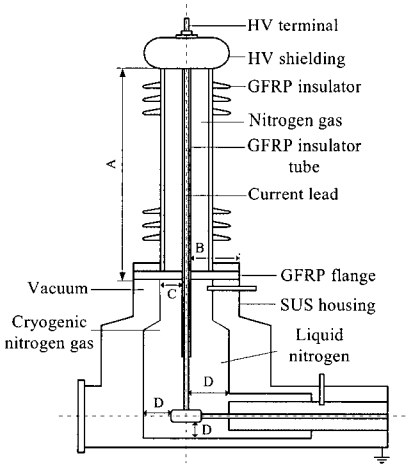

Fig. 1. Insulation structure of a HTS cable termination.

In this paper, we investigated the surface discharge characteristics of GFRP in air, CGN_2 and GN_2, and the breakdown characteristics of LN_2, CGN_2 and GN_2 were also carried on.

2. EXPERIMENT

Fig. 2 shows electrode systems to measure surface discharge of GFRP in the air while changing the flashover length *l* of the GFRP when ac voltage and impulse voltage were applied. Fig. 2 (a) and (b) show ring-to-ring and triangle-to-plane electrode systems, respectively. In the triangle-plane electrode system, triangle electrode was made of copper and stainless steel while plane electrode was made of stainless steel.

In order to investigate the surface discharge of the GFRP in the GN_2, the triangle-to-plane electrode system shown in the Fig. 2 (b) was reused while changing the flashover length *l* of the GFRP when ac voltage was applied under different pressures of 0.1 MPa, 0.2 MPa and 0.3 MPa.

For studying the surface discharge of GFRP in the CGN_2, the triangle-plane electrode in the Fig. 2 (b) was used. And the experimental set-up is shown in Fig. 3. The distance from LN_2 surface to GFRP surface (d_s) is 10 mm and the ac and impulse voltage were applied to electrode system under the changing of the flashover length *l*. In order to investigate the effect of temperature and vapour-mist density of CGN_2 on flashover voltage, the distance d_s were set to be 10, 30, 50, 100, 130 and 150 mm for 10, 30 and 50 mm of flashover length *l* under ac-applied voltage.

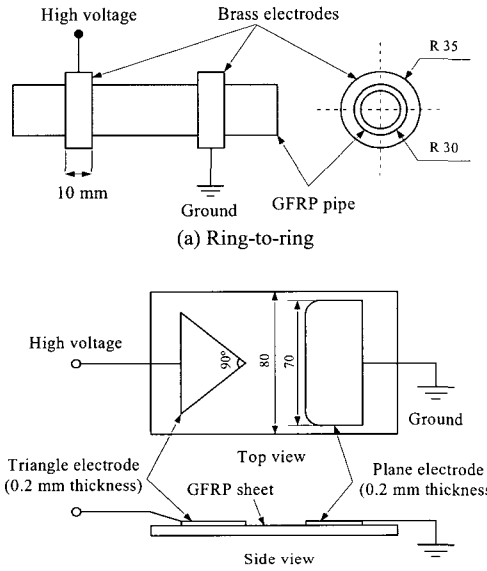

Fig. 2. Electrode system for testing surface discharge of GFRP in air.

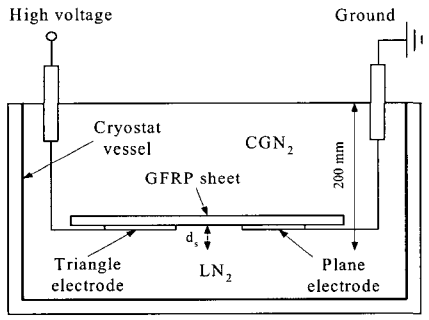

Fig. 3. Experimental set-up for testing surface discharge of GFRP in CGN_2.

The breakdown characteristics of LN_2, GN_2 and CGN_2 and were experiment with sphere-to-plane and sphere-to-plane electrode systems as illustrated in Fig. 4. In LN_2 case, the ac and impulse voltage were applied to electrode systems. In order to study the influence of sphere electrode's diameter to breakdown voltage of LN_2, the diameter of sphere was set to be 3, 5, 10, 19, 30, 38 and 50 mm with the electrode gap d are 1, 2, 3 and 4 mm. In GN_2 case, ac voltage was applied to electrode systems under the pressure of 0.1 MPa, 0.2 MPa and 0.3 MPa. In CGN_2, ac voltage was applied to electrode systems with the distance from liquid nitrogen surface to gap axis d_s was set to be 10 mm as shown in Fig. 5. For investigating the effect of temperature and vapour-mist density of CGN_2 on breakdown voltage, d_s were set to be 10, 30, 50, 100, 130 and 150 mm for 1, 5, 10 and 20 mm of electrode gap d.

Ac breakdown test was carried out according to standard method. The test samples were subjected to a slow ac ramp (1 kV/s) one by one until breakdown occurred [6]. In case of impulse test, the step-up method was used. Firstly, a voltage estimated to be 70 % of breakdown-voltage value was applied to a test object. The voltage was then increased in steps of 4 kV until breakdown occurred. For both of ac and impulse test, the breakdown test was repeated 10 times for each flashover length and electrode gap to obtain an average value of flashover and breakdown voltage.

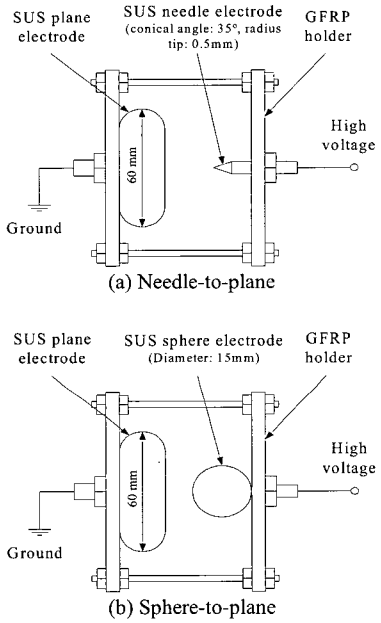

Fig. 4. Electrode system for testing breakdown voltage of GN_2 and LN_2.

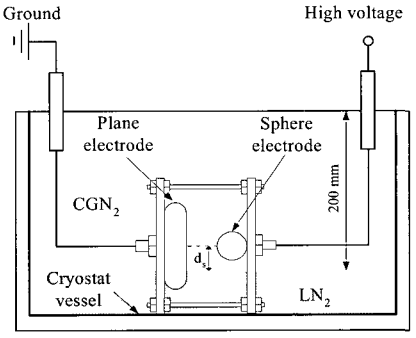

Fig. 5. Electrode system for testing breakdown voltage of CGN_2.

3. RESULTS AND DISCUSSION

3.1. Surface discharge characteristics

Fig. 6 shows the flashover voltage (V_F) of GFRP in the air as a function of flashover length (l). As shown in this figure, ac V_F increases non-linearly with increasing l while impulse V_F increases linearly with increasing of l. The impulse V_F is much higher than ac V_F. In addition, V_F is slightly affected with the material of electrode (copper or stainless steel) and the shape of electrode or electric field configuration of electrode system (ring-to-ring or triangle-to-ring) because the surface properties of GFRP have a strong effect to V_F. The V_F-l relationships are given by

- For impulse

$$V_F = 7.13l + 7.35 \text{ (Triangle-to-plane)} \quad (1)$$

$$V_F = 6.19l + 23.78 \text{ (Ring-to-ring)} \quad (2)$$

- For ac

$$V_F = 9.26l^{0.78} \text{ (Triangle-to-plane)} \quad (3)$$

$$V_F = 9.65l^{0.74} \text{ (Ring-to-ring)} \quad (4)$$

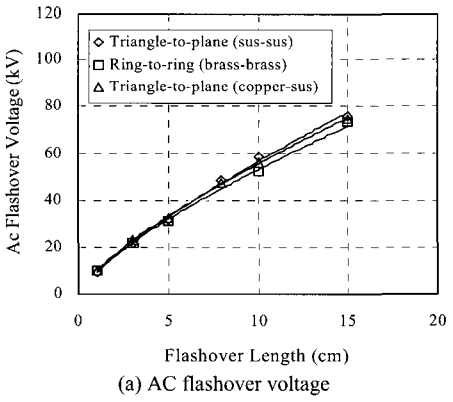

(a) AC flashover voltage

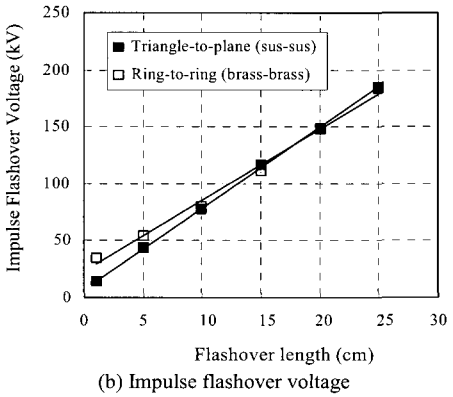

(b) Impulse flashover voltage

Fig. 6. Flashover voltage versus electrode length of GFRP in air.

The V_F of GFRP in the GN_2 is shown in Fig. 7. It is obvious from this figure that V_F increases non-linearly with increasing l and increases as pressure increase. There exists a clear difference in V_F among 0.1 MPa, 0.2 MPa and 0.3 MPa of pressure as l becomes larger in value. The reason is considered that as l has small value, the effect of corona at the tip of triangle electrode is stronger than that of pressure. Although V_F is dependent on pressure, this dependence becomes weaker as pressure is over 0.2 MPa. The V_F as a function of l under the effect of pressure are expressed by

$$V_F = 7.89l^{0.67} \text{ (0.1 MPa)} \quad (5)$$

$$V_F = 11.3l^{0.74} \text{ (0.2 MPa)} \quad (6)$$

$$V_F = 15.46l^{0.67} \text{ (0.3 MPa)} \quad (7)$$

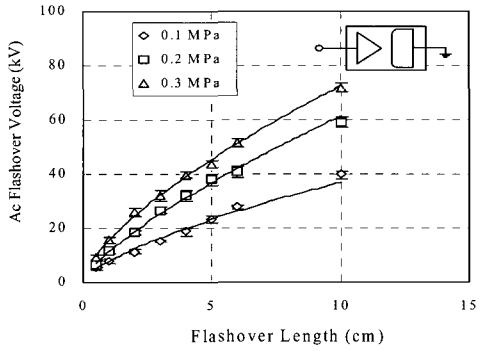

Fig. 7. Flashover voltage versus electrode length of GFRP in GN_2.

Fig. 8 shows the relationship between the V_F and l of GFRP in CGN_2. It is evident that the impulse V_F is higher than ac V_F and the ac V_F increases linearly with a rise of l while impulse V_F is non-linearly proportional with the increase of l. However, the impulse V_F first increases quickly with increasing of l and then it increases slowly as l is over 20 cm. The formulas that show the dependence of the V_F on l are given by

$$V_F = 5.34l + 2.8 \text{ (For ac, with 1 cm} \le l \le \text{10 cm)} \quad (8)$$

$$V_F = 34.64l^{0.48} \text{ (For impulse, with 1 cm} \le l \le \text{20 cm)} \quad (9)$$

$$V_F = 61.89l^{0.3} \text{ (For impulse, } l \ge \text{20 cm)} \quad (10)$$

The dependence of V_F on distance from liquid nitrogen surface d_s is shown in Fig. 9 with the flashover length l is set to be 10, 30 and 50 mm. As shown from this figure, V_F increases with increasing of l and decreases with rising of d_s accordance with well-fitted inverse power law

$$V_F = Ad_s^{-n} \quad (11)$$

Where, A: constant
n: power indices.

The reason for d_s dependence of V_F is considered that d_s increases will make the increase of temperature and decrease of vapour-mist density of CGN_2 [7].

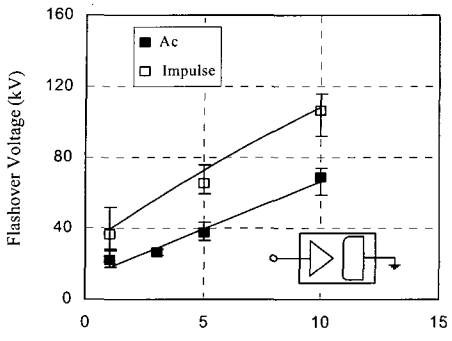

(a) Flashover voltage

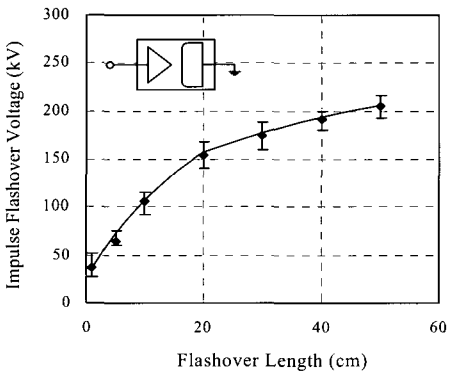

(b) Impulse flashover voltage

Fig. 8. Flashover voltage versus electrode length of GFRP in CGN_2.

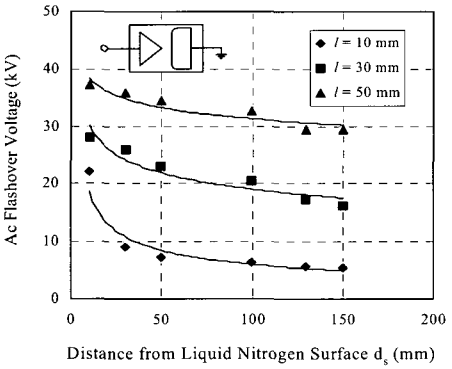

Fig. 9. Flashover voltage of GFRP in CGN_2 as a function of distance from liquid nitrogen surface to GFRP surface.

3.2. Breakdown characteristics

Fig. 10 shows the breakdown voltage V_B of LN_2 as a function of electrode gap d. In both case of electrode systems, V_B increases nonlinearly as d increases and impulse V_B always higher than ac V_B. However breakdown characteristics of needle-to-plane electrode are nearly parallel while breakdown characteristic of impulse V_B is much steeper than that of ac V_B in sphere-to-plane electrode. The reason is due to (1) electric field configuration and (2) corona discharge. It means that the sphere-to-plane has quasi- uniform electric field while needle-to-plane has non-uniform field, so the corona discharge at the tip of needle electrode is stronger than that of sphere electrode. V_B as a function of d are given by

- For needle-plane electrode

$$V_B = 11d^{0.44} \text{ (Ac)} \tag{12}$$

$$V_B = 29.3d^{0.31} \text{ (Impulse)} \tag{13}$$

- For sphere-plane electrode

$$V_B = 46.9d^{1.1} \text{ (Ac)} \tag{14}$$

$$V_b = 28.3d^{0.57} \text{ (Impulse)} \tag{15}$$

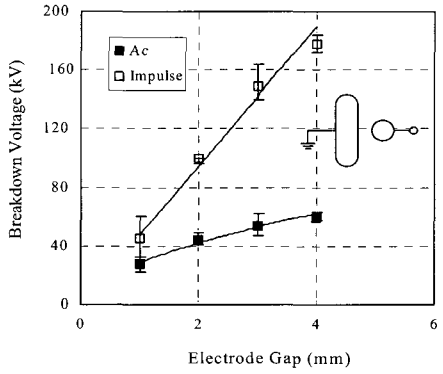

(a) Sphere-to-plane

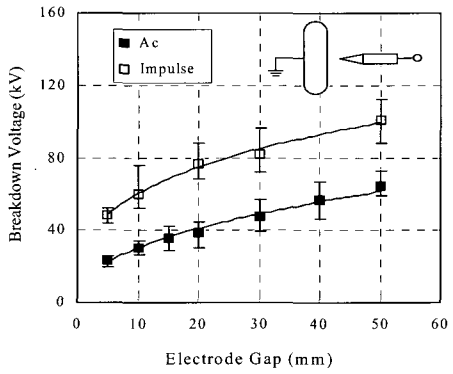

(b) Needle-to-plane

Fig. 10. Breakdown characteristics of LN_2.

The dependence of V_B of LN_2 on the diameter of sphere electrode is exhibited in Fig. 11 (a) with d = 1, 2, 3 and 4 mm. In this figure, the solid lines represent the V_B-d characteristics while the dotted line shows the highest value of breakdown voltage V_{BH} as a function of sphere electrode D. For each value of d, V_B gets the highest value V_{BH} at an

only finite value of D because of the effect of stressed electrode area and stressed liquid volume [8]. Fig. 11 (b) shows V_{BH} and D as a function of d and these relationship functions are indicated by

$$V_{BH} = 12.79d + 13.2 \quad (16)$$

$$D = 2.43e^{0.69d} \quad (17)$$

The relation between V_{BH} and D can be derive from these formulas above as follow

$$V_{BH} = 18.6\ln(D) - 3.26 \quad (18)$$

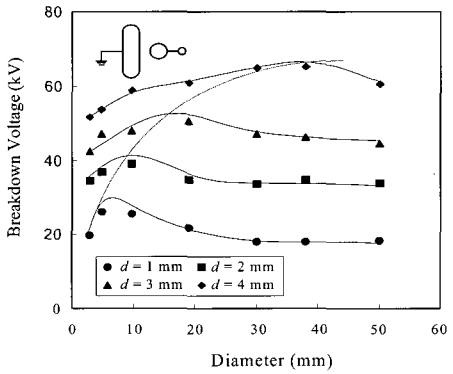

(a) Breakdown voltage as a function of sphere diameter

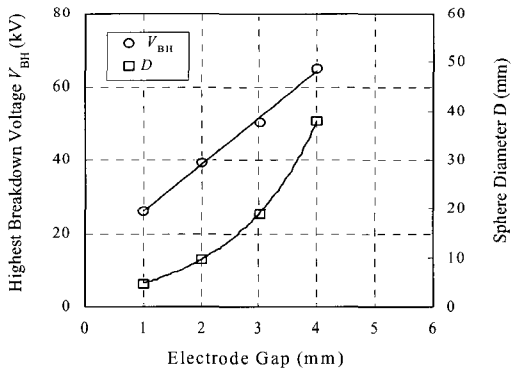

(b) Highest breakdown voltage and sphere diameter as a function of electrode gap

Fig. 11. Effect of sphere diameter on breakdown voltage of LN_2.

Fig. 12 shows the breakdown voltage V_B of GN_2 as a function of electrode gap d under the effect of 0.1 MPa, 0.2 MPa and 0.3 MPa of applied pressures. As shown in this figure, V_B increases non-linearly with the increase of d and GN_2 pressure. However, the pressure dependence of V_B is clearer as d gets larger value in the needle-plane because the effect of corona at the tip radius of needle electrode on V_B becomes weaker in comparing to the pressure effect as d becomes larger. In addition, the effect of pressure on V_B is lesser as the pressure is over 0.2 MPa in sphere-to-plane electrode. However, the effect of pressure on V_B is still stronger as the pressure is over 0.2 MPa in needle-to-plane electrode case due to the fact that the rise of pressure will constrain the corona discharge at the tip of needle electrode and leads to increase breakdown voltage V_B. V_B-d relations are given by

- For needle-plane electrode

$$V_B = 5.84d^{0.8} \text{ (0.1 MPa)} \quad (19)$$

- For sphere-plane electrode

$$V_B = 18.63d^{0.37} \text{ (0.1 MPa)} \quad (20)$$

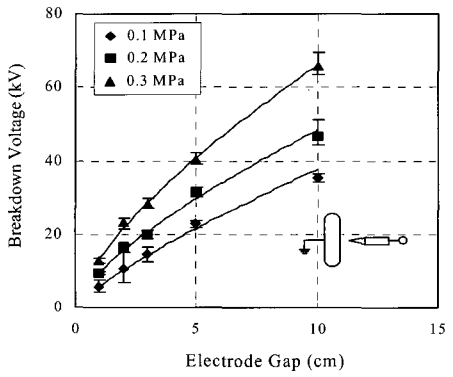

(a) Needle-to-plane

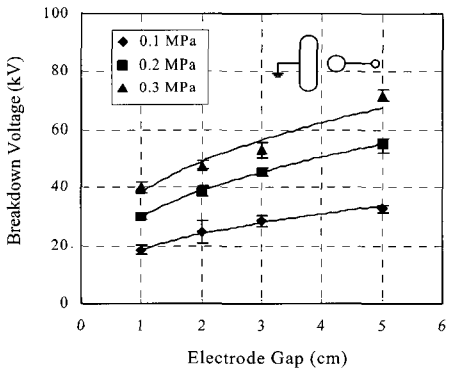

(b) Sphere-to-plane

Fig. 12. Breakdown voltage as a function of electrode gap in GN_2.

Fig. 13 shows V_B of CGN_2 with sphere-plane and needle-plane electrode as a function of d. It is seen from this figure that V_B has a linearly proportional with rising d. However, V_B and standard deviation of V_B is much larger for sphere-to-plane electrode.

$$V_B = 0.72d + 8.65 \text{ (Needle-to-plane)} \quad (21)$$

$$V_B = 1.16d + 20.74 \text{ (Sphere-to-plane)} \quad (22)$$

The effect of distance from liquid nitrogen surface d_s on V_B is illustrated in Fig. 14. As shown in this figure, V_B decreases with increasing d_s in accordance with the inverse-power law as shown in formula 11; thus, the closer is the top surface of LN_2 to the gap, the higher is V_B. The reason is considered that the vapor-mist density of CGN_2 gradually falls and temperature of CGN_2 rises as d_s increases [7]. The d_s dependence of V_B becomes larger as d get higher value because the effect of corona onset on V_B is lower in comparing with the effect of the change of temperature and vapour-mist density as d increases.

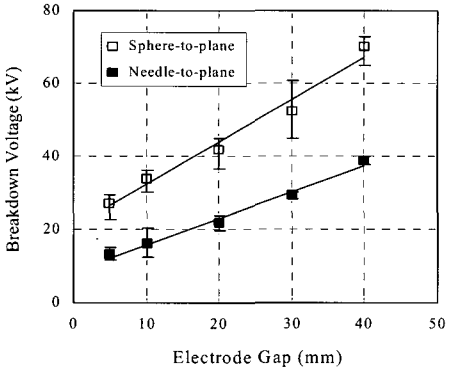

Fig. 13. Breakdown voltage a as function of electrode gap in CGN_2.

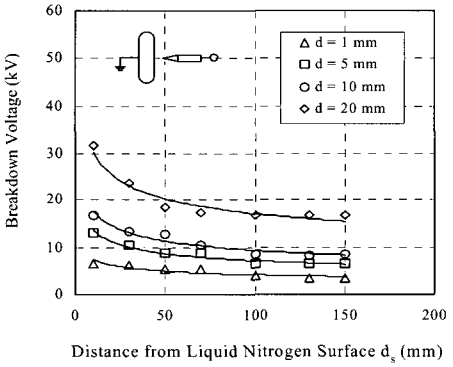

(a) Needle-to-plane

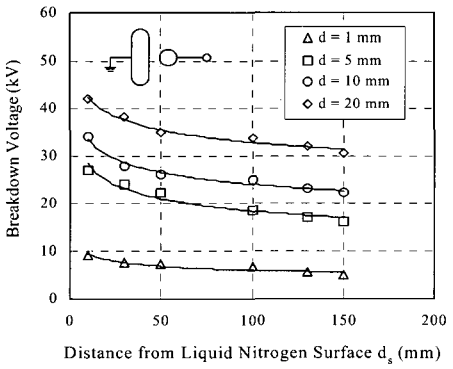

b. Sphere-plane

Fig. 14. Breakdown voltage of GFRP in CGN_2 as a function of distance from liquid nitrogen surface to gap axis.

4. CONCLUSIONS

A basic study on breakdown characteristics of insulators for insulation design of HTS termination was performed and the following conclusions can be drawn:

The flashover voltage of GFRP deeply depends on the flashover length, insulating media, types of applied voltages, pressure, temperature and vapour-mist density of the gas but slightly depends on materials of electrode, shape of electrode, electric-field configuration.

The breakdown voltage is strongly affected by electrode gap, kind of insulator, the shape of electrode, electric-field configuration, pressure, kinds of applied voltages, temperature and vapour-mist density of the gas.

However, it is necessary to perform experiment with larger flashover length, larger electrode gap and higher pressure for surface discharge characteristics of GFRP and breakdown characteristics of LN_2, CGN_2 and GN_2, respectively, in order to well-understood surface discharge characteristics of GFRP and breakdown characteristics of LN_2, CGN_2 and GN_2 leading to make the basic data for insulation designing of termination of HTS cable.

ACKNOWLEDGMENT

This research was supported by a grant from Centre for Applied Superconductivity Technology of the 21st Century Frontier R&D Program funded by the Ministry of Science and Technology, Republic of Korea.

REFERENCES

[1] A. Mansoldo, M. Nassi, and P. Ladie, "HTS Cable Application Studies and Technical/Economical Comparisons with Conventional Technologies," World Congress on Superconductivity, Houston, pp 129-138, 1998.

[2] D. Politano, M. Sjostrom, G. Schnyder, and J. Rhyner, "Technical and Economical Assessment of HTS Cables," IEEE Transaction on Applied Superconductivity, vol. 11, no. 1, pp. 2477-2480, March 2001.

[3] J. Gerhold, and T. Tanaka, "Cryogenic Electrical Insulation of Superconducting Power Transmission Lines: Transfer of Experience Learned from Metal Superconductors to High Critical Temperature Superconductors," Cryogenics 1998 38(11), pp. 1173-1188, 1998.

[4] Y. Minami, C. Suzawa, S. Isojima, S. Nayaga, S. Chigusa, N. Hayakawa, and H. Okubo, "Discharge Characteristics on the Surface for Solid Insulator in Liquid Nitrogen," Proceeding of 13th International Conference on Dielectric Liquids (ICDL, 1999), 99. 474-478, Japan, July 1999.

[5] T. Shimonosono, S. Nagaya, T. Masuda, and S. Isojima, "Development of a Termination for the 77 kV-Class High Tc Superconducting Power Cable," IEEE Transaction on Power Delivery, vol. 12, no. 1, pp. 33-38. January 1997.

[6] ASTM D 149, "Standard Test Method for Dielectric Breakdown Voltage and Dielectric Strength of Solid Electrical Insulating Materials at Commercial Power Frequencies".

[7] H. Goshima, T. Suzuki, N. Hayakawa, M. Hikita, and H. Okubo, "Dielectric Breakdown Characteristics of Cryogenic Nitrogen Gas above Liquid Nitrogen," IEEE Transactions on Dielectrics and Electrical Insulation, vol. 1, no. 3, pp. 538-543, june 1994.

[8] H. Goshima, N. Hayakawa, M. Hikita, H. Okubo, and K. Uchida, "Area and Volume Effects on Breakdown Strength in Liquid Nitrogen," IEEE Transactions on Dielectrics and Electrical Insulation, vol. 2, no. 3, pp. 376-384, June 1995.